HOPKINS STUDENT WIND ENERGY TEAM

Technical Design Report

Johns Hopkins University
Collegiate Wind Competition 2021

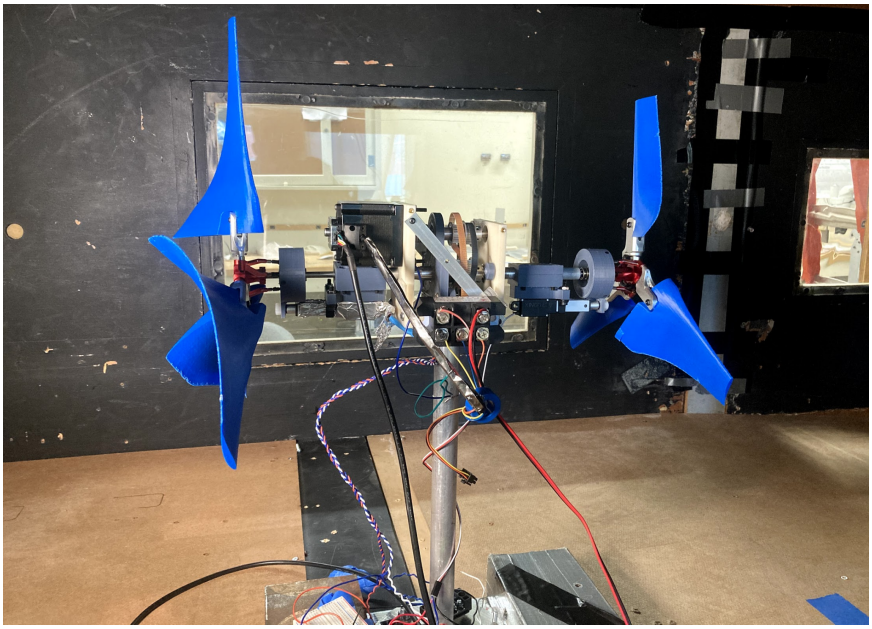

Generator Team:
Willa Grinsfelder (Generator, Structures Lead)
Zach Galvarro

Aerodynamics Team:
Owen Friesen (Aerodynamics Lead)

Structures Team:
Kathy Cao, Ebuka Ezekwesili,
Evan Latourrette-Ghez, and Isaac Lee

Electronics & Controls:
Annika Torp (Electronics & Controls Lead)
Shivanie Ally, Caitlyn Bernhard, Eleni
Daskopoulou, Yared Kokeb, and Daniel Okereke

With Assistance from Prof. Nathan Scott, PI

JOHNS HOPKINS UNIVERSITY

COLLEGIATE WIND COMPETITION
U.S. DEPARTMENT OF ENERGY

Table of Contents:

1.0 Executive Summary

For our inaugural entry to the Collegiate Wind Competition, the JHU team aimed to maximize the efficiency of a turbine that complies with the space requirements of the competition. To do so, we developed a novel dual-rotor counter-rotating turbine design that allows us to extract more power from a limited swept area than a comparable single-rotor design. Dual rotor turbines have a higher theoretical efficiency than single-rotor variants, with a maximum efficiency of 81.4% compared to the 59.3% Betz Limit [1].

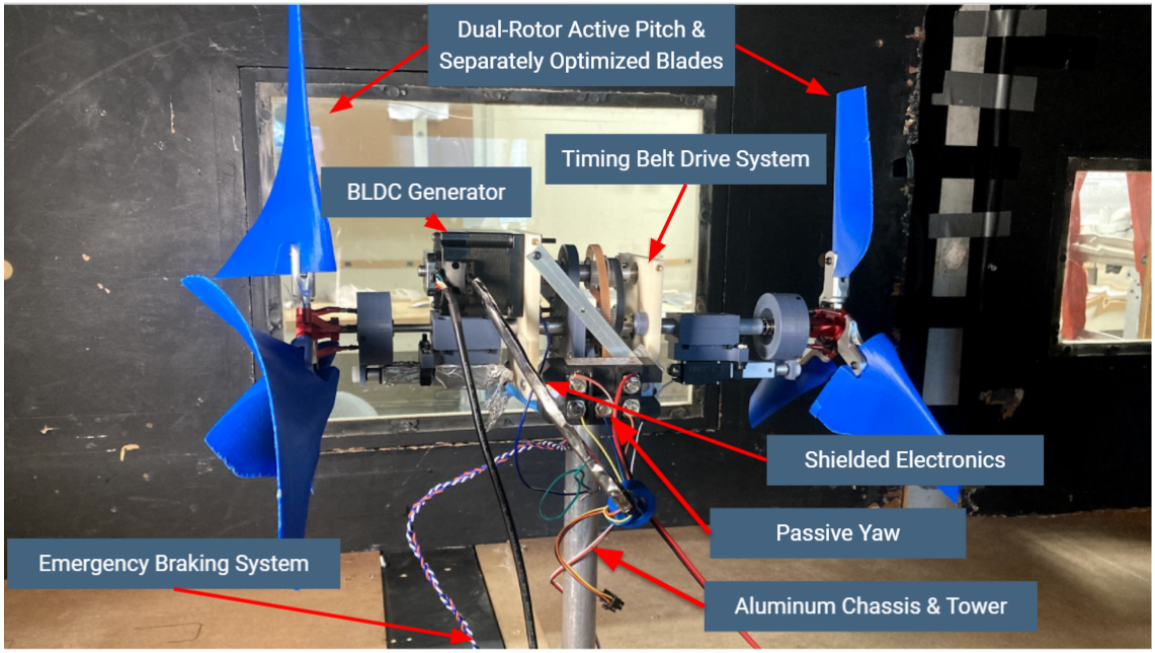

Figure 1: Overview Schematic of our Final Prototype.

Our blades are derived from the S1210 airfoil which was originally designed for RC aircraft. This airfoil is well suited to our low-Reynolds number application [2]. We separately optimized the front and rear sets of blades for the applicable flow conditions. We then 3D printed the blades from ABS and smoothed them with acetone to even out the surface finish.

Our controls employ two variable pitch mechanisms, one for each rotor, to control and brake the turbine. This system uses two linear actuators mounted to our chassis, which, with intelligent programming, minimizes power consumption while allowing us greater control over turbine performance.

We use a timing belt transmission system to combine the mechanical power from the two rotor shafts and step-up the generator shaft speed. By stepping up the shaft speed of the generator, we are able to better achieve the maximum efficiencies of both our blade design and generator. We selected a commercial brushless 3-phase motor to drive as a generator by using the weighted average of generator power production over competition wind speeds.

In an attempt to improve upon prior art, we decided to design a safety system that can brake the turbine without a functioning microcontroller by using low-level logic gates and other simplistic electrical devices, with the goal of improving robustness. This design struggled with the multiple conditions under which it had to execute different functions (which is why others in the past have preferred controlling

braking with a microcontroller); however, this system could be hugely successful with improvements in future years.

Finally, we built a tower and chassis using a combination of machined metal parts and 3D printed parts to improve the overall manufacturability of our design in highly uncertain times, when the availability of machining equipment and the consistency of our access to lab spaces were changing with the global pandemic.

The peak efficiency measured in testing our turbine was 21.8%. This efficiency was lower than the theoretical levels predicted in literature for dual-rotor counter-rotating wind turbine designs, but we were able to build a working dual-rotor design for this application. In future years we hope to continue developing our counter-rotating wind turbine design with the ultimate goal of breaking through the Betz limit.

2.0 Technical Design

For the 2021 Collegiate Wind Competition, our team was tasked with researching, designing, and building a miniature wind turbine for highly uncertain times. We specifically sought to maximize our turbine's power production between 5 and 11 m/s using novel counter-rotating wind turbine prototype. Individual team members spearheaded the development of our four key subsystems — blades, structure, generator, and electronics — while working from home during the fall semester. In the spring, our team came together to integrate our components and test them in our university's one-meter wind tunnel. The following sections detail the design, analysis, and testing of each of these key sub-components.

2.1 Blade Design

We designed and built our turbine blades to accommodate the unique opportunities and challenges of a counter-rotating wind turbine. For the competition, we developed a pair of rotors with separately optimized blade geometries to match the unique flow conditions present at the front and rear of the turbine. These rotors also work in concert to provide passive yaw control for our system, negating the need for a separate tail. With separate active pitch control systems for each rotor, we are able to tailor the turbine characteristics to produce optimal performance under a wide range of conditions.

2.1.1 Aerodynamic Design

The core of our aerodynamic system is a pair of rotors which, working together, extract mechanical energy from the wind. Both rotors are based off of the S1210 airfoil, shown in Figure 2, which we chose for its high C_L/C_D ratio at low Reynolds numbers ($Re < 100{,}000$).

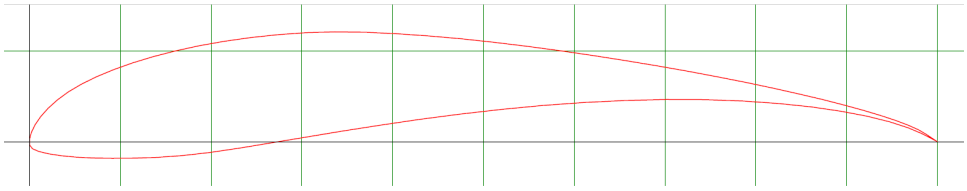

Figure 2: The S1210 airfoil [3].

The S1210 airfoil was originally designed for low-Reynolds number applications in RC aircraft, and is therefore well suited for use in small length scales [2]. Because of these favorable properties, this airfoil

has been adopted by a number of research teams for small scale wind turbines, and it was our choice for the 2021 competition [2, 4].

Once we selected our airfoil, we constructed our blade geometries in QBlade. The overall dimensions of our blades were informed by our yaw system (see below). To accommodate passive yaw, we designed our front blades with a diameter of 35 cm and our rear blades with a diameter of 45 cm. Our active pitch hub had a 3.5 cm radius, allowing an overall blade length of 14 cm for the front blades and 19 cm for the rear blades. Our blades also experienced different flow conditions because of turbulence and their different geometries. Through an iterative process based on the analysis described below, we determined that our front blades are subject to flow at Re = 90,000 and our rear blades are subject to flow at Re = 70,000.

The last key input for our QBlade optimization was the tip-speed ratio (TSR). Based on iterative testing with our generator, we chose to use a TSR of 3 for both rotors for our final set of blades. With our geometry and flow parameters established, we were able to use the Betz optimization process in QBlade to determine an ideal twist and chord length array for the two sets of blades. We could then conduct further aerodynamic analysis in QBlade and extract STL files with the blade geometry for further structural design in Solidworks.

2.1.2 Aerodynamic Analysis

To perfect this blade geometry, we conducted both computational analysis and iterative testing. This was essential to account for the unique flow conditions present in a dual-rotor system, which is not natively supported by QBlade nor well-researched. We did most of our computational analysis using QBlade's native lifting-line theory (LLT) function, shown in Figure 3, which provides more detailed flow data than blade element momentum (BEM) analysis without the computational cost of computational fluid dynamics (CFD). To model our system, we conducted two separate sets of analysis. First, we modeled our front rotor at the chosen wind speed and TSR. We then extracted the velocity field 45 cm behind that rotor to model the wake that the rear rotor experiences. In Excel, we could process this data to obtain the average flow velocity in the swept area of the rear rotor, and use that as the input for a second LLT simulation to model the rear rotor. This simulation provided useful data for design, but its accuracy was limited by the use of the single x-velocity variable to model the interaction between the two systems, as well as the fact that we could not model the counter-rotation of the rear rotor this way.

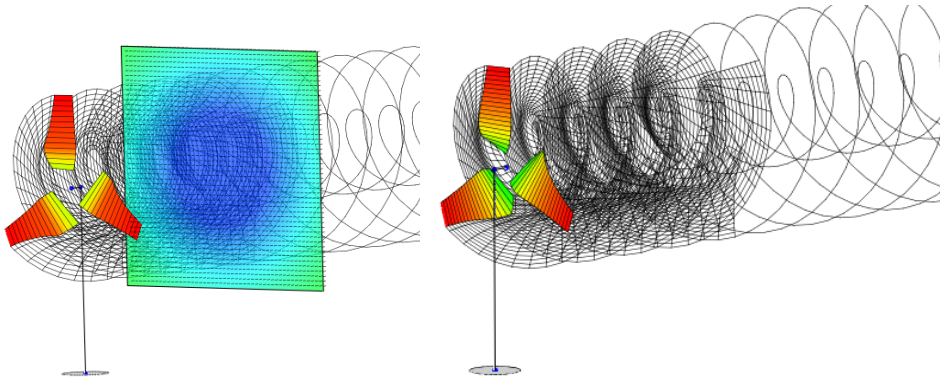

Figure 3: LLT simulation of the front (left) and rear (right) rotor with the velocity plane behind the front.

The lifting-line theory model predicted an 11% average drop in the flow velocity as a result of the front rotor. This decreases the efficiency of the rear rotor, but the additional rotor still significantly improves the overall coefficient of performance of the system. As shown in Figure 4, we predicted a total power output of up to 75 W with the dual rotor system at 11 m/s.

	Front	Rear	Combined
Inlet Velocity (m/s)	11	9.8	11
Power (W)	37	38	75
C_p	0.47	0.41	0.58

Figure 4: An example of the results of the LLT simulations, at 11 m/s.

This simulation likely has significant error, because of the aforementioned simplifications in the LLT model and the fact that the model does not incorporate feedback from the generator. As a result, we sought a lot of physical testing to validate our models and refine our optimizations.

Over the course of the year, we went through 15+ iterations of the blade design, shown in Figure 5. This allowed us to test our blades independently and in combination with various generators.

Figure 5: A series of blade prototypes produced and tested throughout the year.

During these tests, we gathered wind speed, power, and RPM data from our data acquisition system, which allowed us to finetune the flow characteristics and TSR we used for our optimization, as discussed above. Our final testing yielded a pair of power coefficient (Cp) vs. TSR curves shown in Figure 6, which illustrates that our peak performance is obtained at higher TSRs. We were able to control the TSR with our load and blade pitch. This shows that we did a good job of matching the TSRs of the two rotors, with the rear rotor operating at only slightly higher TSRs than the front one. As expected, the experimental power coefficient did not reach our ideal values from the LLT simulations but showed significant improvement as we continued to iterate, reaching an average of 21.8% under our final set of conditions.

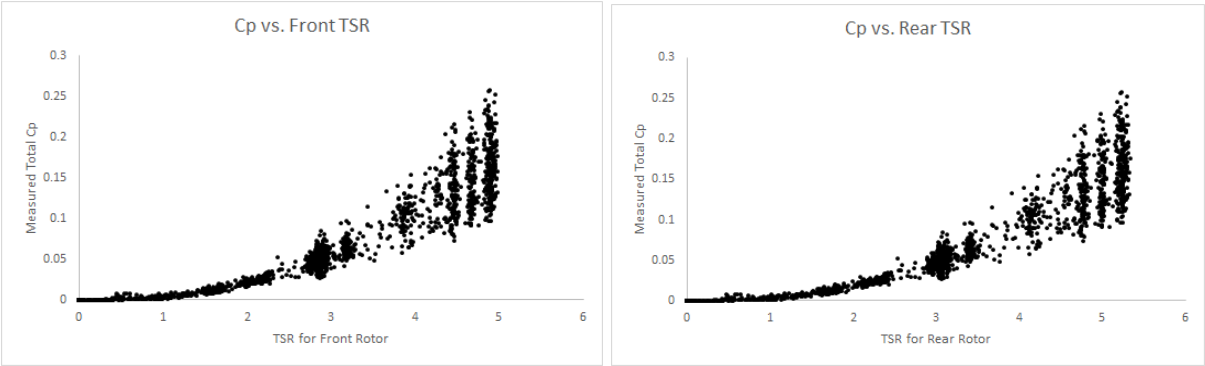

Figure 6: Cp vs. TSR plots for our front (left) and rear (right) rotors during testing at 11 m/s.

2.1.3 Yaw Design & Analysis

We achieved passive yaw through a size differential between our two rotors and a yaw bearing, which allowed our full system to self-center in the flow. The objective for the passive yaw system is to have the turbine respond to yaw rates of 180° per second at wind speeds between 6 m/s and 13 m/s. The transient response of the yawing turbine was modeled using MATLAB and a series of simplifying assumptions.

The net torque acting on the turbine over time was calculated as the sum of the torque from the drag on the front blades, the torque from the drag on the back blades, and the rolling frictional torque in the two bearings at each timestep. We used the SKF model to approximate the rolling frictional torque [5]. The net torque was used to derive the angular acceleration, angular velocity, and yaw angle over time.

Figure 7 shows the transient response of the yawing turbine for yaw angles of 1° and 179° at a wind speed of 9 m/s. The results suggest that the yaw system is able to respond to yaw rates of 180° per second at wind speeds between 6 m/s and 13 m/s. Additionally, as shown in Figure 7, a larger initial yaw angle is predicted to take the turbine longer to equilibrate at 0°. In practice, we saw the turbine equilibrate more quickly than predicted by the model, likely because of additional rolling frictional torque. Note that this model cannot accommodate initial yaw angles of 90° and 180° since the net torque would be calculated as zero for those angles.

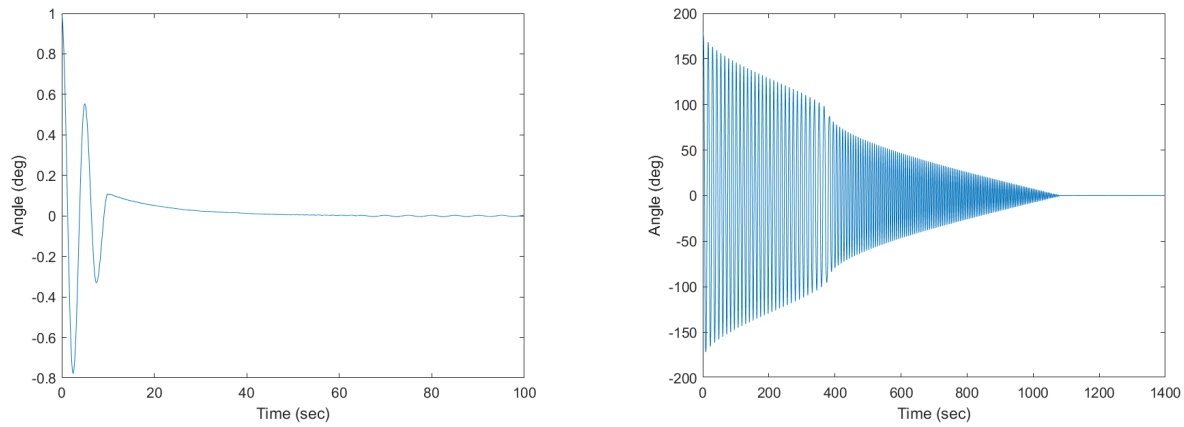

Figure 7: Transient response of yaw angle for initial yaw angle of 1° (left) and 179° (right) at 9 m/s.

2.1.4 Rotor Hub Design

For our rotor hub, we chose to use a modified hub from a JCZK 300C RC helicopter, shown in Figure 8, to achieve active pitch control. We epoxied a linear bearing in line with the shaft to limit the pitch control to one degree of freedom and ensure that the three blades on each rotor pitched together. This pitch system is attached to our Actuonix L12 linear actuator with a 3D printed coupler to obtain precise control.

Figure 8: JCZK 300c Rotor Hub [6]

In order to mount the blades to the rotor hub, we imported the blade geometry from QBlade to Solidworks. We could then add in appropriate mounting geometry that lined up with the neutral plane. Therefore, when the active pitch system is at a neutral position, the blades are pitched appropriately.

All of our blades and other 3D printed parts were 3D printed from ABS with a solid infill. We chose ABS for its ease of printability and relatively high strength and heat tolerance compared to other 3D printed materials. Parts that did not require high degrees of accuracy were printed on a Qidi X-plus home 3D printer. More accurate parts for the blades and chassis were printed on both a UPrint SE Plus and a Stratasys F370 in university-managed facilities, still from ABS. We post-processed the blades in an acetone vapor bath to ensure a smooth surface.

Figure 9: Assembly drawing of turbine structure including rotor and blade shaft and support structures (green) and major chassis and tower components (red).

2.2 Structural Design

The objective of the structural design of our wind turbine is to adequately support all wind turbine components in both parked conditions and the maximum operating conditions of wind speeds of 22 m/s. We also designed for a small frontal area of the chassis in order to minimize power losses over the chassis. Finally, we included a thrust and radial ball bearing assembly to passively yaw the turbine.

The major loading conditions on the turbine are a thrust load on both sets of blades of 5.3 lbf per rotor in wind speeds of 22 m/s, a maximum rotor rotational speed of 2500 rpm, and a bending moment of 50 N·m at the base of the turbine. In the “parked” case both the front and rear blades of the turbine are feathered. The frontal area of the feathered blades is 12% of the area of the blades during operation. This indicates that the turbine’s major mode of failure will be due to loads manifesting during operation. The minimum safety factor in the design is 12.5 in the back rotor shaft due to fatigue loading conditions. A complete table of calculated safety factors is available in Appendix A.2.

2.2.1 Rotor Shaft Supports

The rotor shaft support assembly consists of the two 6 mm 416 Stainless Steel rotor shafts supported by machined 6061-T6 aluminum support arms. This design was chosen for the smaller form

factor it allowed us with the dual-rotor design, as well as ensuring quick and easy assembly of key parts. after our team noticed significant walking in earlier bearing mount assemblies during testing. In addition, the support arm allows the rotor to be assembled to the final chassis with ease.

2.2.2 Chassis

The chassis was designed out of three 6061-T6 machined aluminum brackets and four cross braces. The objective of the design is to support the bending moment from the cantilevered rotor support arms and accurately position the transmission assembly while minimizing frontal area. The chassis brackets clamp to the passive yaw bearing housing using four M5 screws for ease of subsystem assembly and disassembly. The stresses in the chassis brackets were modeled in ANSYS. For testing, the turbine chassis was fabricated from 3D Printed ABS so that we could perform fit checks and quickly adjust our design. The final prototype of the turbine structure is designed to be professionally machined from 6061 Aluminum.

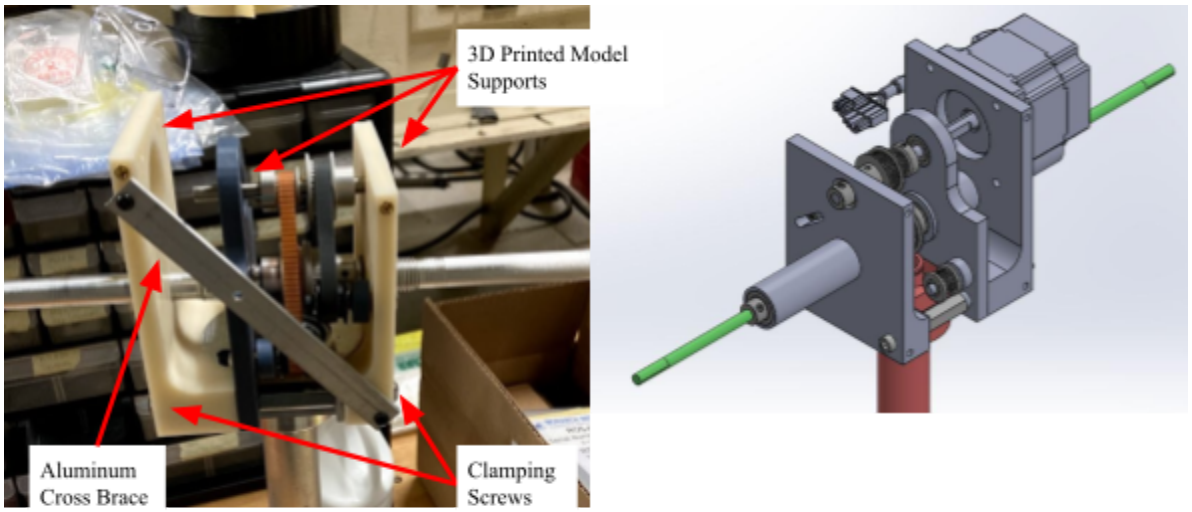

Figure 10: Annotated image of the major components of the chassis structure when test assembly produced (left) and CAD model of completed assembly sans aluminum cross bars (right) to the turbine tower.

2.2.3 Passive Yaw Bearing Assembly

The design objective for the passive yaw bearing assembly is to minimize friction in the yawing assembly while ensuring our design is robust enough to withstand unpredictable vibrational loading of the turbine blades. In addition, the design was completed such that the cross sectional area projected on the flow is minimized, which minimizes power losses due to impingement on the flow. The design uses a 3220JR Tapered Roller Bearing and a 60/22 deep groove ball bearing to allow for free rotation of the turbine in variable loading conditions. The mounting assembly is designed such that the tapered roller bearing takes the

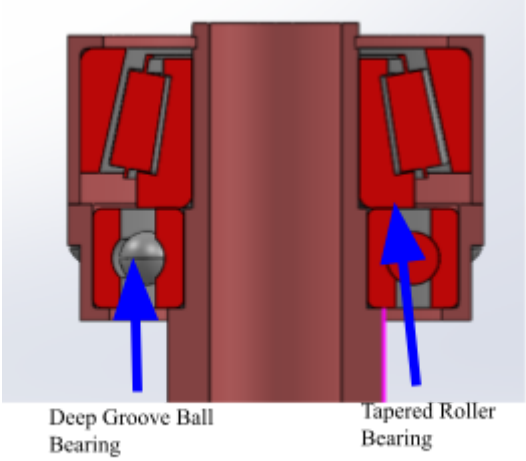

Figure 11: Cross Section of Yaw Bearing Assembly

majority of the axial load, and the roller bearing resists any bending moment caused by the thrust on the turbine blades.

2.2.4 Brazed Aluminum Joint at Turbine Base

The design objective for the tower and base plate is to create an easily replicable assembly that withstands at least 50 N·m of bending moment. Since the height of the wind tunnel on the JHU campus is significantly smaller than the height of the competition wind tunnel, we needed to design a turbine tower that could easily be swapped depending on our circumstances. To accomplish this goal our team minimized machining operations for the 6061-T6 aluminum tower and used brazing to permanently fasten the base plate to the tower. This allowed our team to avoid threading or milling bolt holes into the base plate after turning it to size and maintained the strength of our joint. We found that the brazed aluminum joint on the 1" diameter tower withstood more than 70 N·m of force in laboratory testing, indicating that the design was appropriate for the competition requirements.

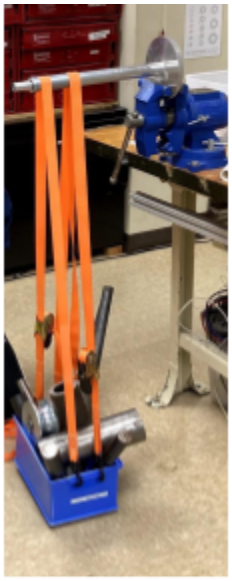

Figure 12: Brazed aluminum tower in laboratory testing.

2.3 Generator Design

The objective of our generator design is to maximize the weighted power performance of our turbine between wind speeds of 5 and 11 m/s.

2.3.1 Numerical Simulation

The operating parameters of the generator were determined using a simplified actuator disk model of a dual rotor wind turbine [1]. The optimal generator rotational speed was defined by the blade TSR and wind speed. The maximum torque on the generator was derived from the mechanical power equation for a rotating shaft and the theoretical maximum power harvestable from the wind. A transmission system was included in the generator design to step up/down the input speed and torque from the rotor blades to the generator. The main purpose of the transmission system is to combine the mechanical power from the two sets of turbine blades. To evaluate the optimal transmission ratio and generator combination, power production was estimated over the operating range of wind speeds given incremental changes in the transmission ratio. The weighted score for generator and transmission performance was calculated based on the Collegiate Wind Competition's scoring rubric [7]. The generator and transmission combination with the highest weighted score was chosen for our generator design.

2.3.2 Simulation Validation

The simulation of generator performance was verified using an in-house dynamometer and Maxon RE 50 generator, one of the first generators our team identified as a viable option. While we discovered a load mis-match between our turbine blades and generator which led us to revisit alternative generator options, the dynamometer testing allowed us to use the MATLAB generator performance simulation with confidence in our generator selection.

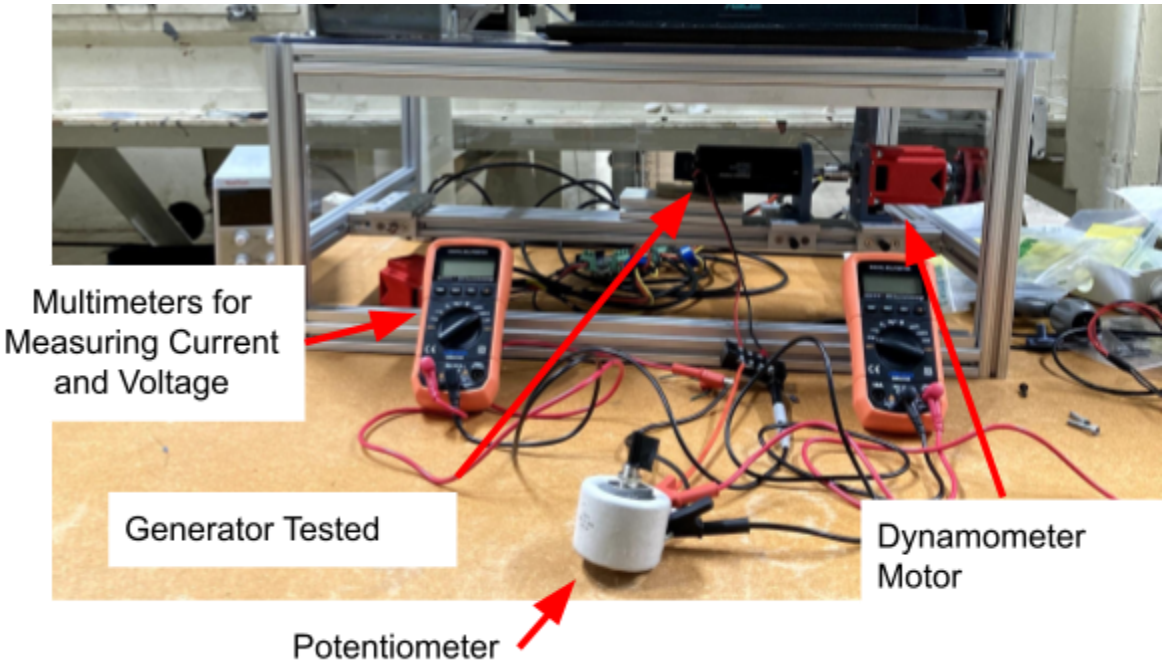

Figure 13: Dynamometer assembly used for validating generator numerical simulations.

2.3.3 Selected Generator and Predicted Performance

A range of brushless DC motors and brushed DC motors' power performance were used to identify the optimal combination of motor constants for generator selection. To achieve a maximum generator efficiency, our team aimed to select a generator that would spin quickly, demand low torque from the drive shaft, and minimize copper losses in the windings of the generator. Parameters that played a role in our final design included motor speed constant, motor speed-torque constant, terminal resistance in motor windings, and cogging torque when available from data sheets. For the competition this year our team decided to use the Lin Engineering BL23E22-02 brushless DC motor. The optimal transmission for both startup wind speed and power curve performance was a transmission ratio of 0.8 from the front blades to the generator shaft. This translated to an increase in rotational speed of 1.25, and a decrease in torque of 0.8 from the front shaft to the generator. The following table outlines the key parameters that this generator satisfies.

Table 1: Outline of generator predicted performance over range of operating wind speeds.

Condition	Lin Engineering Generator Performance
Startup Wind Speed between 2.5 and 5 m/s	Predicted to startup at 4.5 m/s and produce 3.83 W
Maximize Power Curve Performance between 5 and 11 m/s	Predicted to achieve a maximum power production of 23.3 W at 11 m/s, and total weighted performance score of 46 out of 50

2.4 Transmission Design

The objective of the transmission system in the wind turbine design is to efficiently combine the mechanical power of the two rotor blades into a single input for the generator. For the turbine this year, our team decided to use a timing belt system as our transmission system. The timing belt system was ideal for our team as we experimented with varying transmission ratios, chassis designs, and blade-generator combinations because built-in tensioning mechanisms allowed for ease of adjustment while keeping overall costs low.

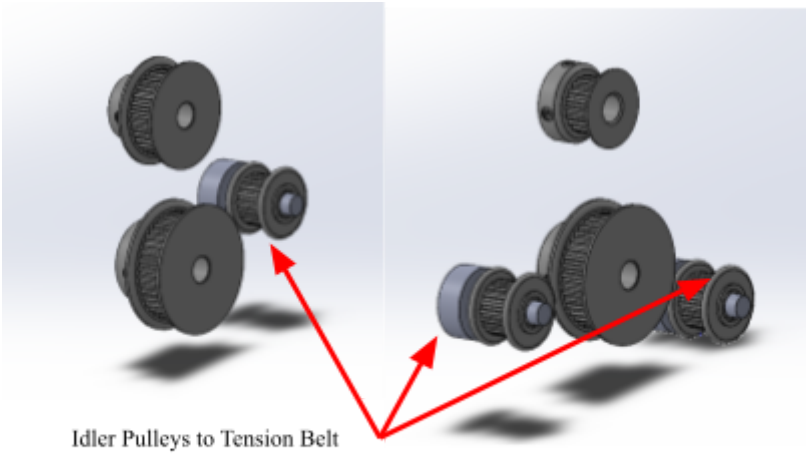

Figure 14: The front rotor pulley assembly (left) and the back rotor pulley assembly (right) including the idler pulleys with adjustable position.

The MXL series timing belt pulleys were used for their small size and weight. The gear ratios used in the final design were based on the generator modeling simulation, as well as the assumed aerodynamic relationships between the front and back rotor. The following table outlines the gear ratios:

Table 2: Tooth counts on pulleys in wind turbine transmission system.

	Tooth Count on Rotor Shaft Pulleys	Tooth Count on Generator Shaft Pulleys
Front	40	32
Back	40	20

Thus the ratio of the front rotor shaft speed to the generator shaft speed was a ratio of 1.25, and the ratio of the front rotor shaft speed to the back rotor shaft speed was 1.2. Both timing belts were manufactured with Kevlar tensioning chords, with a maximum yield strength of 1865 N, well above the calculated maximum tension of 39 N for this design [8].

2.5 Electrical Design

The purpose of the electrical system is to regulate and optimize the power produced by the generator. To accomplish this, the electrical system is controlled by a single microcontroller unit (MCU), which pitches both sets of blades, reads sensor and state data, and controls the variable load. The electronics design also features a safety system that has the intention of improving robustness by braking the turbine without the input or processing power of the MCU.

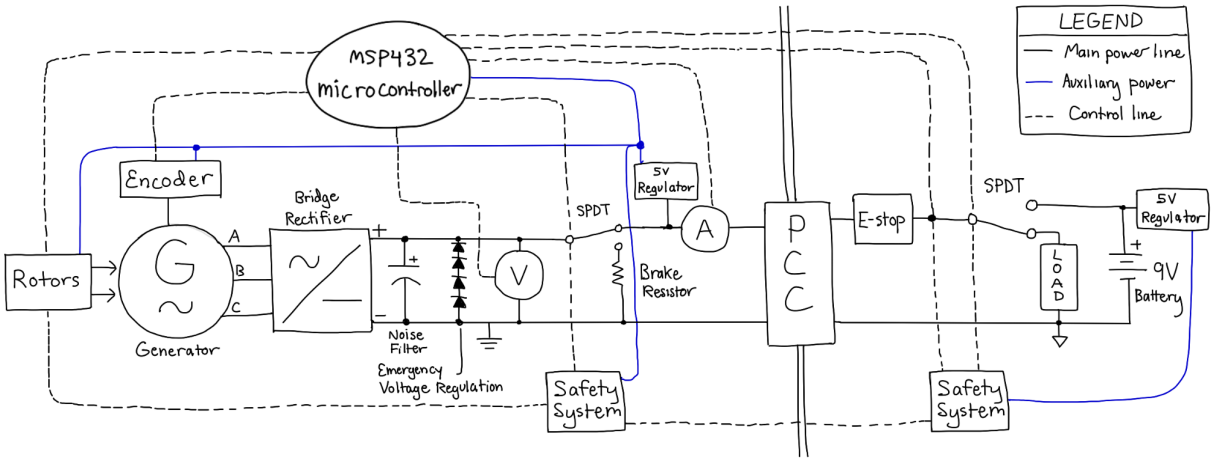

Figure 15: Overview of the electronics system. Full circuit diagram in Appendix 2.

The Texas Instruments MSP432 LaunchPad was chosen as our MCU for its low power consumption and because it is Arduino-compatible. We chose early on to only use one MCU with the goal of reducing complexity and the chance for error. The MCU measures the generated voltage through a voltage divider and the current using a current shunt monitor breakout board. Both of these measurements are read as an analog input voltage and a rolling average is taken of the last ten measurements to mitigate noise effects, then that average is used by the MCU to make decisions. Generator speed is measured by a quadrature encoder, the signal of which the MCU uses to count the number of rotations in a given time period. The MCU pitches the two sets of blades during normal operation by sending pulse-width modulation (PWM) signals to the linear actuators.

While the goal of only using one MCU to reduce complexity was a good one, this increased our power consumption on the turbine-side of the PCC due to the increased number of optically isolated signals that needed to cross the PCC, and a solution to this problem should be found in future years.

2.5.1 Variable Load

Ahead of the necessary information to choose the appropriate resistor values for a variable load system, we designed one that allowed for up to eight different resistance values, intended for seven different wind speed bins and a startup load resistance. Power resistors are added in parallel to each other with power MOSFETs controlled by the MCU. These resistances would be determined by thorough testing at various wind speeds, blade pitches, and load resistances.

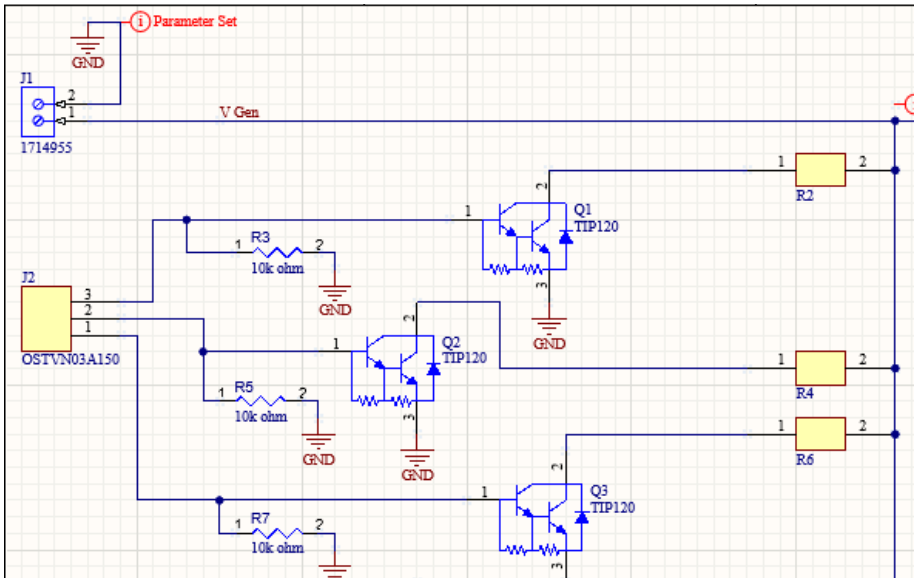

Figure 16: Part of the variable load circuit -- signals come in from the turbine side (left of the image) and control MOSFETs that add power resistors in parallel (right of the image)

2.5.2 Voltage Regulation

We only anticipate reaching ~30V in testing, however, should the generated voltage reach 45V as measured by the sensors, the control system will pitch the blades to reduce the power output of the turbine. In case of a control malfunction at high voltages, we also have four 12V diodes in series that span the output of our bridge rectifier, which would short the generator at 48V.

2.5.3 Power Smoothing

The power output of the three-phase generator was modeled using MATLAB. The necessary capacitance was selected based on the stability criteria of the competition rules and regulations. A smoothing capacitor was included in series with the full-wave bridge rectifier to ensure power stability over the full operating range of the generator. The minimum capacitance was selected based on the calculated frequency of the rectified power output to be 30 mF. To account for any unexpectedly low frequency operating points, a smoothing capacitor with a value of 50 mF was chosen for our design.

2.5.4 Safety System

The goal of our safety system design is to brake the turbine independently of whether or not the MCU is functioning for improved safety and robustness upon prior art. This is achieved by “reading” states at different points in the circuit, and using low-level logic gates to actuate the braking of the turbine. Figure 17 below shows the “safety” part of the circuit, with unnecessary information removed to better illustrate how the system functions.

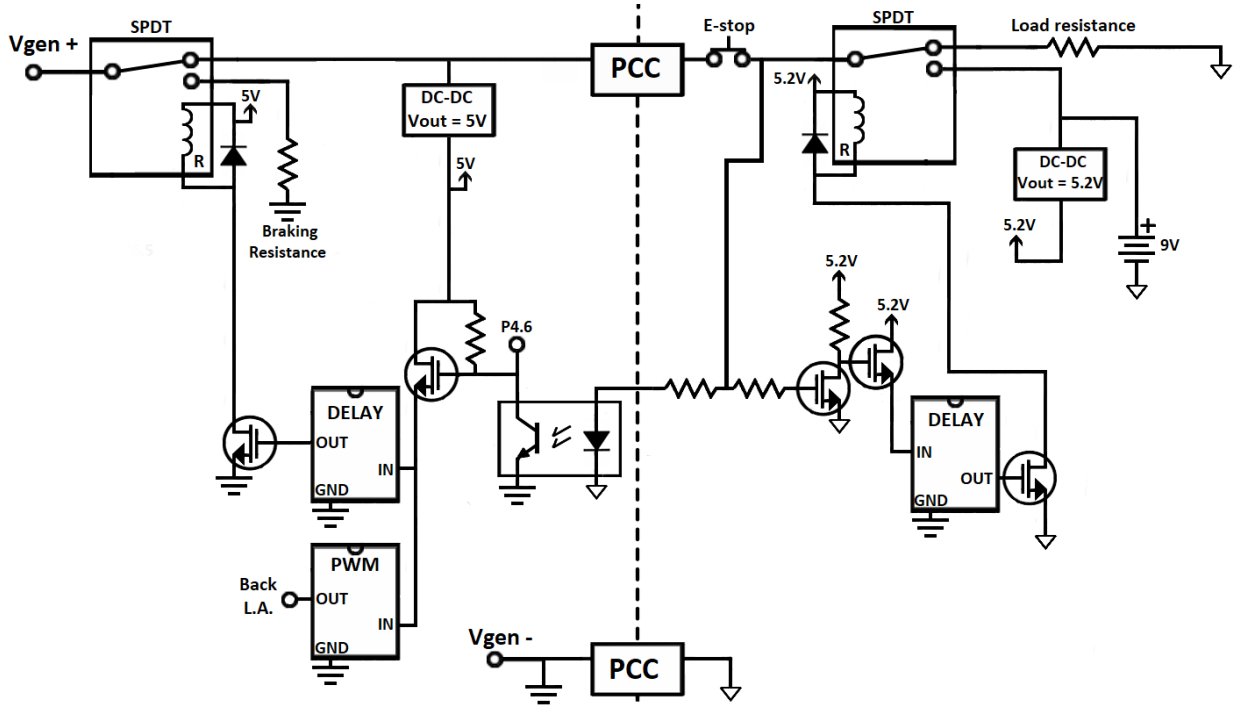

Figure 17: The safety system with no microcontroller intervention (extraneous information removed).

For our prototype and testing setup, we are able to place our emergency stop button in series with the PCC, as our button is rated to ~460V and 10A, and our generator is not rated to produce more than 1.6A.

The system works by converting the generated voltage at a node on the load side of the PCC down to a logic-level 5V, and using this "HIGH" or "LOW" condition to begin the braking process. If this node is "LOW" (load disconnect or E-stop button press), the logic gates on either side of the PCC begin the braking process -- on the turbine side, the rear rotor blades pitch to a predetermined braking angle from a PWM signal generated by a 555 timer IC. On either side of the PCC, a separate 555 timer circuit begins a delay for a latching relay. The turbine side relay resets first, and disconnects the generator from the main power line and to a braking power resistor. The load side relay resets second and disconnects the main power line from the variable load, and switches it to a backup battery pack. Meanwhile, the rear blades have been pitched and the turbine is slowing to a halt. With the selection of an appropriate battery pack (we are using 6 AA batteries in series), the system can wait indefinitely like this, until the emergency stop button is unpressed or the PCC reconnected. Once this happens, the MCU is operating off of the backup battery, and will begin a restart, which is described in the Control Model Analysis section. Importantly, there is an additional, small latching ("first run") relay on the load side that is reset before a testing session begins, which prevents the safety system from triggering upon the first startup (every other startup within a testing session is presumed to be from a purposeful brake). See Appendix 2 for the full circuit diagram.

2.6 Control Model

As mentioned previously, we chose the MSP432 LaunchPad for its low power consumption, and this board remained on the turbine-side of the PCC. The MCU has two primary decision-making loops and three operational states it must traverse. Upon powering on, it must first go through the loop within the *STARTUP* state, which it will only exit if it has enough power for the safety system to run properly

(assumed to be at or below 5 m/s). It will then enter into the *NORMAL OPERATION* state, where it optimizes or limits the power to the load. It's here that the MCU also monitors whether or not the circuit has entered into the *SAFETY* state, in which the MCU does nothing.

Figure 18 shows the finite state machine that indicates how the MCU navigates the information it reads in during *STARTUP*, and Figure 19 shows how it operates in *NORMAL OPERATION* or *SAFETY*. The specifics of the change conditions between states and the microcontroller functions of each state are in Table 4.

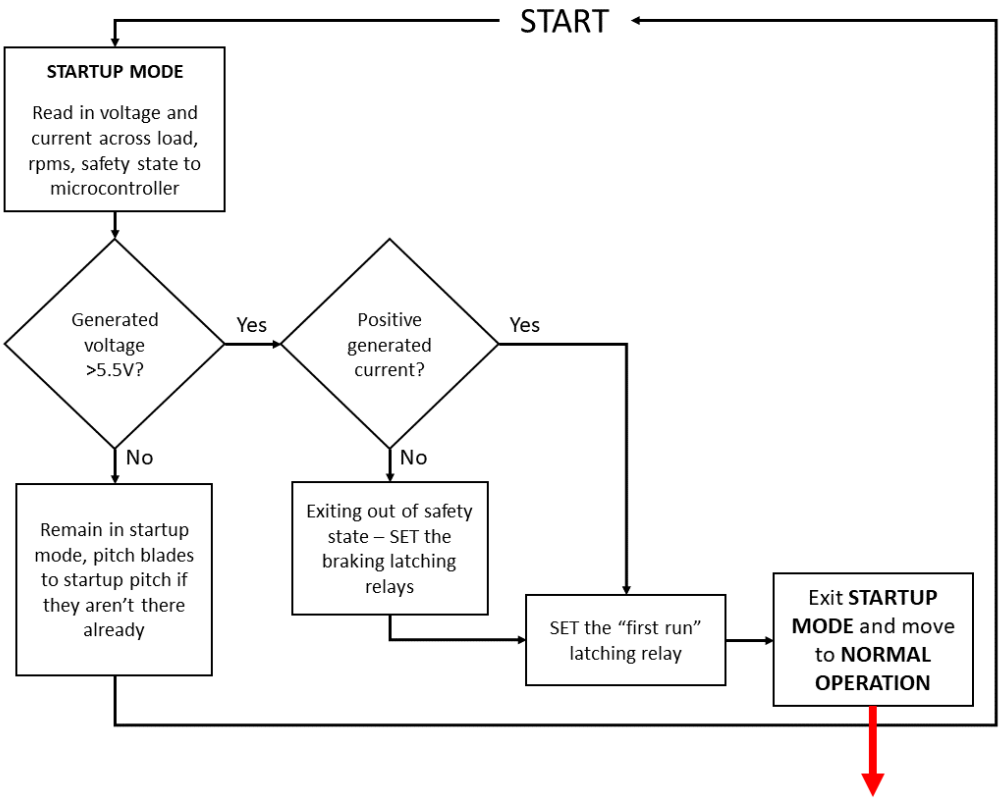

Figure 18: Finite state diagram within *STARTUP* state. The system cannot enter the safety state from startup, which complies with testing requirements assuming startup at or below 5 m/s.

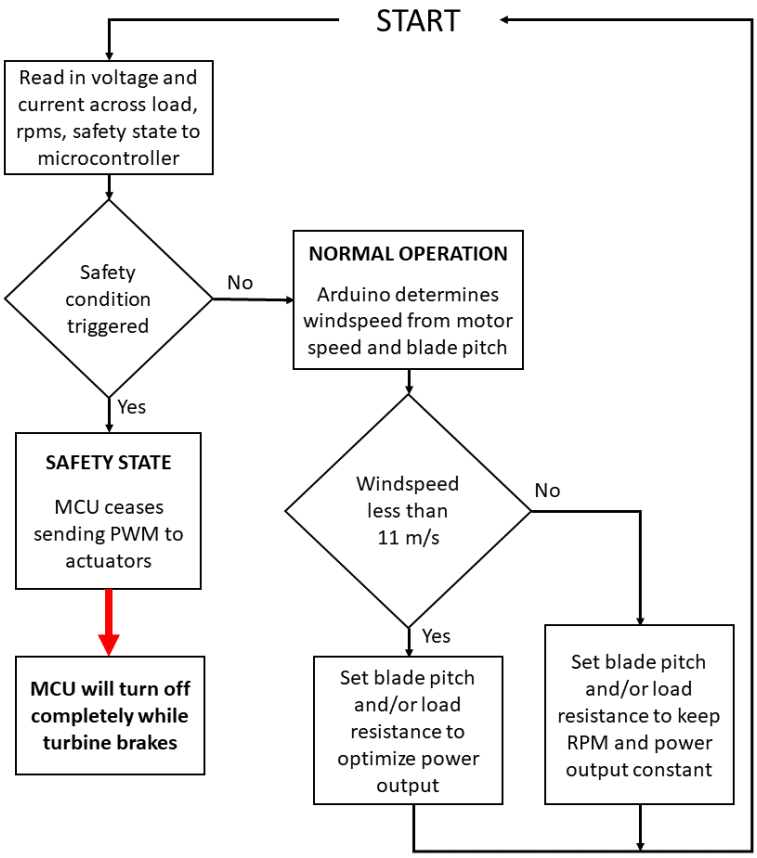

Figure 19: Finite state diagram for the *NORMAL OPERATION* and *SAFETY* states. The MCU has no function during the *SAFETY* state.

Table 3: List of states, their functions, and their change conditions.

State	Description of State Functions	Change Conditions
Startup	• Starting state when MCU powers on • Pitch blade to startup if necessary • Set all latching relays before exiting	Go to normal operation when voltage is >5.5V and there is positive current

Normal Operation	• Read in voltage, current, motor speed, and safety condition
	• "Calculate" wind speed and make decisions based upon it
	• If below 11 m/s:
	  ○ Optimize power output by pitching blades and changing variable load
	• If above 11 m/s:
	  ○ Limit power output by pitching blades
		Go to safety state when safety condition is read in as true

Safety	• Cease PWM output to linear actuators	MCU turns off completely when the turbine is braked

In order to optimize the power curve of the turbine, the MCU must estimate the wind speed by using known power curve data from testing of the final turbine. It takes the two blade pitches and encoder data and compares it to data hard-coded into the MCU program through a series of if/else statements. If the current blade pitches and load setting are not the optimal ones for the current wind speed, the MCU will change those settings.

3.0 Testing

For our final validation testing, our team used the Corrsin Wind Tunnel, a low speed wind tunnel located on the Johns Hopkins campus seen in Figure 20. We were able to characterize the flow in the tunnel to test our turbine at wind speeds of 2.5 m/s to 13 m/s. Our final prototype successfully produced positive power at a wind speed of 4.5 m/s, meeting the startup condition. The turbine was also able to yaw effectively in the flow, and continue producing positive power throughout the yawing events simulated. We collected power and encoder data at multiple speed bins, and collected the results seen in Figure 21 to characterize the system.

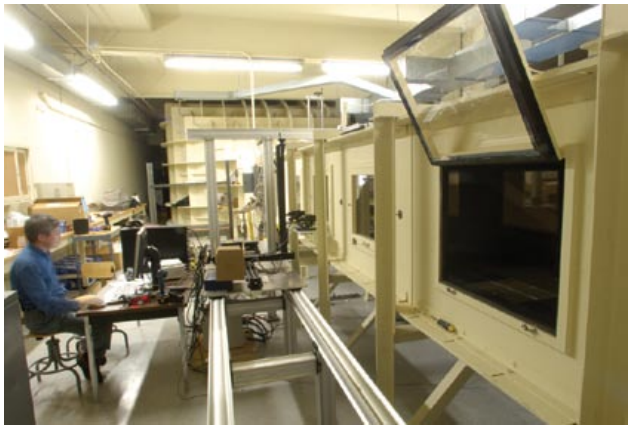

Figure 20: Corrsin Wind Tunnel

3.1 Commissioning Checklist

- ❑ Assemble all mechanical components of the wind turbine outside of the wind tunnel
- ❑ Place the turbine in the center of the wind tunnel, threading wire from the base of the turbine through appropriate channels
- ❑ Secure the turbine to the wind tunnel (using metal weights in the Corrsin wind tunnel, or fasteners provided by the Collegiate Wind Competition)
- ❑ Attach electrical leads from the positive and negative generator terminals to the turbine electronics
- ❑ Attach electrical leads for the linear actuators (5V, signal, ground) to the turbine electronics
- ❑ Attach electrical lead from the turbine electronics ground to the turbine tower
- ❑ Attach electrical lead from the turbine tower to the earth-grounded wind tunnel structure
- ❑ Confirm continuity of all electronics using digital multimeter, beginning with grounds
- ❑ Turn on the power to the wind tunnel, and switch it on to its lowest wind speed (2.5 m/s)
- ❑ Adjust wind speed as needed for operation and testing (in the JHU Corrsin wind tunnel)

3.2 Results

Our system produced positive power at a range of wind speeds above 4.5 m/s. We compared our results to those from some previous competitions, and found that our power curve was comparable to a mid-range performance, with a maximum average output of 21 W at 11 m/s. We did have some significant

problems with noise in our system, which we corrected in generator design by adding a smoothing capacitor to our system.

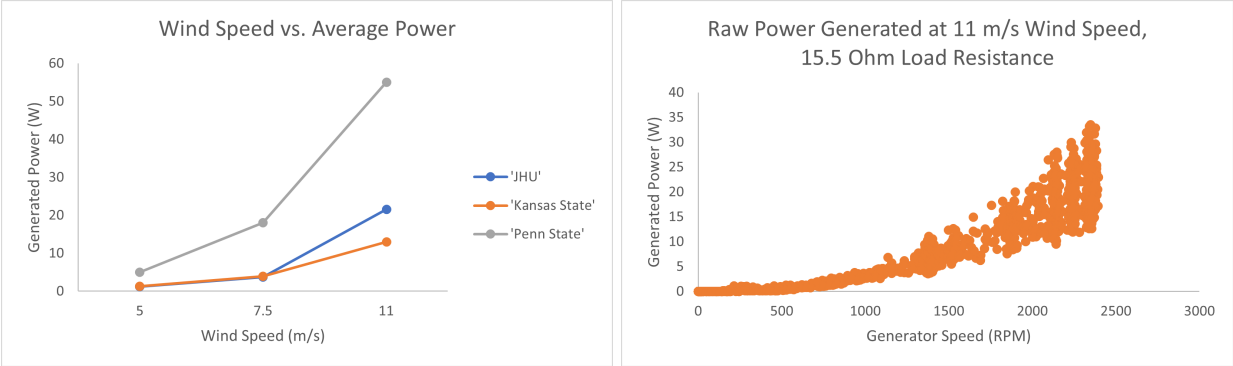

Figure 21: Our team's performance compared to other teams in 2019 (left) and our noise issue (right).

4.0 Conclusion

This year, our team successfully designed, built, and tested a working miniature counter-rotating wind turbine in a distributed fashion. While we did not meet all of our goals for our system's performance, we met the key competition specifications for size, safety, and design. With a cut-in wind speed below 5 m/s and a power coefficient of up to 21.8% at 11 m/s we would expect to perform well if the competition was able to include a testing component this year. As our school's first entry to the Collegiate Wind Competition, we believe we have set a solid foundation with an innovative design that future years can build on to achieve even better performance.

5.0 Enumeration of Influence of Previous Design Reports

As a first-year team, we pulled extensively from previous design reports to gain a foundational understanding of miniature wind turbine designs. From the winning teams in 2019 and 2020, Penn State University and California Maritime University, we gained an understanding of some of the key off-the-shelf components that exist and are useful in miniature turbine design, including the use of off-the-shelf pitching mechanisms, linear actuators with microcontroller libraries. We also built our dynamometer and generator testing assembly based on previous team's design reports, selected a variable load system based on Penn State's electronics diagram, and adopted the practice of monitoring wind speed and power output using rpms and voltage instead of wind speed sensors. These are a few of the many lessons that our team learned from previous team's reports, and we are grateful that these reports were provided as reference materials.

6.0 Appendices

6.1 Full Circuit Diagram

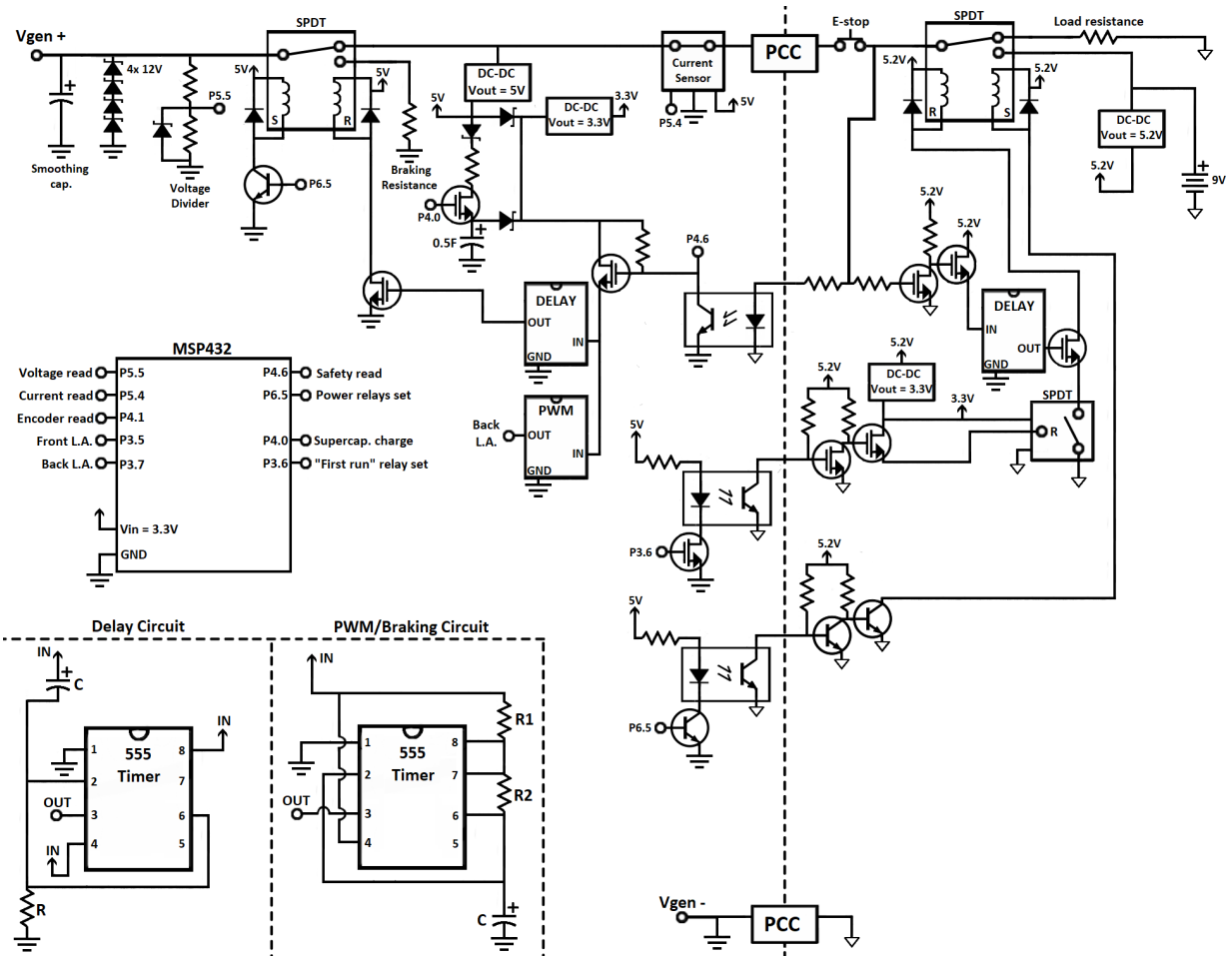

6.2 Table of Safety Factors

A complete table of calculated safety factors in tower design, based on FEA simulations and hand calculations.

Location	Maximum Stress	Calculated Safety Factor
Tower	11.16 MPa	49.4
Braze (tower-base joint)	11.16 MPa	35.84 - 85.13
Base plate	5.7317 MPa	48.52
Front Rotor Shaft	20.1 MPa	17.3575
Back Rotor Shaft	27.9 MPa	12.508
Front Rotor Support Arm	0.89044 MPa	309.72
Front Chassis	1.2284 MPa	224.51
Back Chassis	0.48528 MPa	568.31

7.0 References

[1] Sundararaju, Lo, K.H., Metcalfe, R., and Wang, S., 2017, "Aerodynamics and CFD analysis of equal size dual-rotor wind turbine," Journal of Renewable and Sustainable Energy, 9(043305), from https://aip.scitation.org/doi/pdf/10.1063/1.4999500

[2] Chen, S., 2020, "Numerical Investigation of Wind Turbine Airfoils under Clean and Dusty Air Conditions," Ph.D. thesis, Washington University in St. Louis, from https://openscholarship.wustl.edu/cgi/viewcontent.cgi?article=1577&context=eng_etds

[3] "S1210 12%", from http://airfoiltools.com/airfoil/details?airfoil=s1210-il

[4] Singh, R.K., Ahmed, M. R., Zullah, M. A., and Lee, Y. H., 2012, "Design of a low Reynolds number airfoil for small horizontal axis wind turbines," Renewable Energy, Volume 42 66-76, from https://doi.org/10.1016/j.renene.2011.09.014

[5] "The SKF model for calculating the frictional moment." SKF. From: https://www.skf.com/binaries/pub12/Images/0901d1968065e9e7-The-SKF-model-for-calculating-the-frictional-movement_tcm_12-299767.pdf

[6] "JCZK 300C RC Helicopter Parts Main Rotor Head Set" From: https://usa.banggood.com/JCZK-300C-RC-Helicopter-Parts-Main-Rotor-Head-Set-p-1653921.html?cur_warehouse=CN&ID=513344

[7] "US Department of Energy Collegiate Wind Competition 2021 Rules and Regulations" National Renewable Energy Lab, October 9th 2021. From: https://www.energy.gov/eere/collegiatewindcompetition/downloads/collegiate-wind-competition-rules-and-requirements

[8] "Belt and Chain Drives" SDP/SI Catalog. From: https://sdp-si.com/D820/PDFS/Belt-and-Chain-Drives.pdf